NANO LETTERS

pubs.acs.org/NanoLett
Letter

Dual Action Spectroscopy Exposes the Bright and Dark Excitons of Room-Temperature WSe_2

Joseph Wragg,* Luca Bolzonello, Ludovica Donati, Karuppasamy Pandian Soundarapandian, Riccardo Bertini, Seth Ariel Tongay, Kenji Watanabe, Takashi Taniguchi, Frank H. L. Koppens, and Niek F. van Hulst*

Cite This: *Nano Lett.* 2025, 25, 7658−7664

ABSTRACT: While it has long been accepted that the role of momentum dark excitons in the photoresponse of transition metal dichalcogenides (TMDs) is critical, their weak optical signature inhibits their study through conventional means. Here we expose the room-temperature contributions of both bright and dark excitons to the behavior of a TMD, WSe_2, from monolayer to multilayer to bulk. To do so, we present dual action spectroscopy, a photocurrent- and luminescence-detected Fourier-transform excitation spectroscopy scheme, to microscopically map the energy landscape of WSe_2. While bright excitons naturally dominate the luminescence response of the material, dark excitons dominate the current response. Notably, the dark **KK′** exciton is more accessible than the ground state **KΛ**, while current maps reveal a disparity in the diffusivity of the two states. This work provides the basis for a new, current-detected approach to study the dynamics of dark exciton states across different materials.

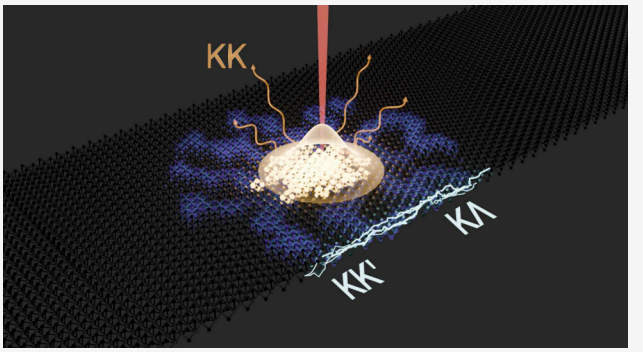

KEYWORDS: *transition metal dichalcogenides, 2D materials, action spectroscopy, energy transport, dark excitons*

The physics of bound electron−hole pairs, or excitons, and their role in energy transfer carries importance across several disciplines of science.[1−3] Their influence on material properties is particularly pronounced in transition metal dichalcogenides (TMDs), a class of two-dimensional materials.[4] TMDs owe their remarkable electronic properties to stable excitons which exhibit binding energies in the region of 0.5 eV.[5−7] The planar nature of these excitons, that are largely confined to individual TMD layers,[8−10] makes them not only ideal candidates for novel optoelectronic devices but also useful platforms for the study of exciton behavior.[11−13] Once an exciton is created, what it does with its energy determines the photoresponse of the material. Short lifetimes[14] followed by radiative recombination of excitons is prevalent in monolayer (ML) TMDs.[5,15] In the multilayer material, specifically for WSe_2 which we study here, this photoluminescence (PL) is diminished.[16−18]

The loss of luminescence efficiency raises the question: what happens to the excitons that go "dark"? The decrease in radiative recombination points to the material's multivalley band structure that induces myriad allowed and forbidden exciton states.[9,19] Such states unlock a new regime of exciton physics in TMDs, where lifetimes move from the pico- to the nanosecond[20,21] and diffusion lengths move from the nano- to the micrometer.[22] Indeed, great effort has gone into understanding these forbidden, or dark, excitons as the significance of their role in the photoresponse of TMDs has become increasingly clear. These efforts include cryogenically emptying the population of higher energy bright states to observe dark exciton PL,[19−26] application of in-[27−30] and out of-plane[31] fields to induce spin state mixing, and nanopatterning of the TMD substrate to induce strain in the material, encouraging recombination of the dark exciton.[32,33] Understanding dark states can inform the realization of valleytronic and spintronic devices with these materials.[34,35]

Here we present dual action spectroscopy, experimentally separating the contributions of dark and bright excitons to the photoresponse of WSe_2 at room temperature. We diagnose the valley of origin of each dark exciton and infer their role in the transport of energy through the material. This is achieved by simultaneously measuring the PL and photocurrent (PC) response of a WSe_2 flake of multiple thicknesses, from the

Received: December 11, 2024
Revised: March 28, 2025
Accepted: March 28, 2025
Published: April 4, 2025

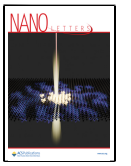

https://doi.org/10.1021/acs.nanolett.4c06349
Nano Lett. 2025, 25, 7658−7664

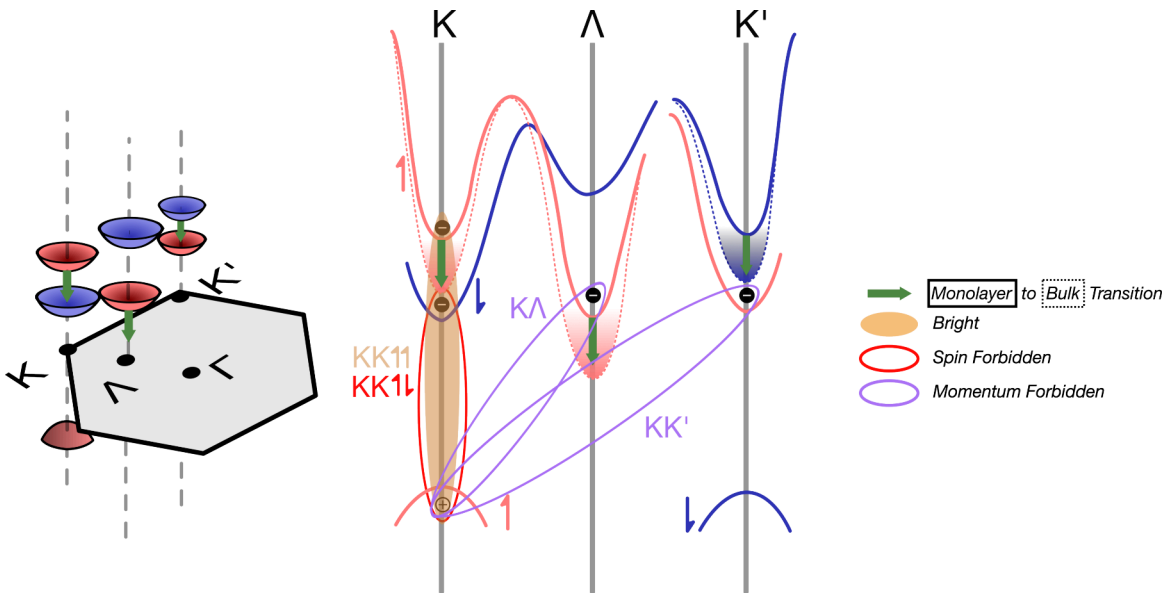

Figure 1. Monolayer to bulk WSe_2, bright to dark excitons. Band structure and corresponding Brillouin zones of monolayer (solid lines) and bulk (dashed lines) WSe_2 using data compiled from refs 9, 10, and 36. The spin states of each band are represented in red and blue, indicating whether a transition between states is spin allowed or forbidden. Notable exciton states are outlined with ellipses. The only allowed transition is bright **KK** shown in orange, which accounts for the observable fluorescence response of the material. All other excitons shown here are forbidden. The ground state of monolayer WSe_2 is the spin-forbidden **K↑K↓** exciton (red hollow ellipses). Moving to the bulk, conduction band relaxation at the **Λ** symmetry point means the momentum-forbidden (purple hollow ellipses) **KΛ** exciton becomes the ground state, while throughout all layers the **KK′** (purple hollow ellipses) maintains its energy shift relative to the VBM, due to offsetting effects of spin relaxation across inverse points in the *k*-space.

monolayer to bulk, to retrieve the spatially resolved excitation spectrum of the TMD through both observation channels. The combination of the two detection mechanisms enables the separation of bright and dark excitons due to their respective dominance in the PL and PC response. Naturally, radiative recombination in the material is representative of the bright exciton response, which is shown in the PL excitation spectrum. Conversely, the more stable, but less abundant, dark excitons are more likely to contribute to the PC generated in the material, that requires exciton diffusion over micrometers. This natural filtering of the bright exciton contribution enables the observation of these dark states that, due to their low yield ($<1 \times 10^{-6}$), evade detection in typical experimental approaches such as conventional absorption and differential reflectance. Probing the excitation spectrum in both domains also offers insight into the states that are directly accessible with optical stimulation instead of those to which the system relaxes as in conventional PL spectroscopy. We hope that the insight we provide can be of use to the community in the design of devices using these materials going forward.

Although many of the plethora of charge and energy carrying states available in WSe_2 at cryogenic temperatures are destroyed by phonons at room temperature, the multivalley form of the TMD's conductance band means that many tightly bound exciton states can still exist. Spin−orbit coupling, as well as weak intralayer dielectric screening, lead to a complex band structure. A heavily simplified version of the diagram, showing the excitonic states that will be relevant for this study, is compiled from the theoretical calculations of refs 9, 10, and 36 in Figure 1.

Across both conductance and valence bands, spin−orbit coupling induces splitting between the two electronic spin states throughout the first Brillouin zone.[37] In the valence band, the splitting is so pronounced (100s of meV[10]) that for the band edge transitions that we are able to resolve here, we only need to consider one spin configuration. For the sake of Figure 1, we show this configuration as spin ↑. There are a number of transitions available to an electron sitting at the valence band maximum (VBM) of the monolayer, located at the ↑**K** high symmetry point. Of these transitions, only one near the band edge is allowed. This is the bright exciton,[29] shown in orange in Figure 1. It is responsible for the large PL response of monolayer WSe_2. The other three transitions shown all represent dark excitons. The first, shown as a hollow red ellipse, is the spin forbidden transition to the ground state of the **K** point. The final two, shown as purple ellipses, are the momentum-forbidden transitions of the electron across the *k*-space, with valleys lying at the **Λ** and **K′** points.

Adding extra layers to the material changes the band structure. Although excitons remain largely confined to a single layer, overlap of the out-of-plane orbital components with neighboring layers relaxes the energy of the conductance band edge across the Brillouin zone.[10] The introduction of new magnetic fields from surrounding layers specifically relaxes the higher energy spin states at the **K** and **K′** points, bringing the two spins close to degeneracy. This shift is indicated by dotted lines in Figure 1. The largest relaxation occurs at the **Λ** symmetry point, which incurs a red shift of ∼200 meV relative to the VBM from its monolayer value. This makes the dark **KΛ** transition the ground state exciton for bulk WSe_2. The shift represents the origin of the PL suppression in multilayer TMDs, as electrons excited into the conductance band from the VBM are far more likely to relax into the energetically lower valleys away from the **K** point, where the corresponding hole remains.

Although defining the shift in the ground state exciton is a useful way of defining the behavior of the semiconductor, all of the valleys across the conduction band can provide a stable

https://doi.org/10.1021/acs.nanolett.4c06349
Nano Lett. 2025, 25, 7658−7664

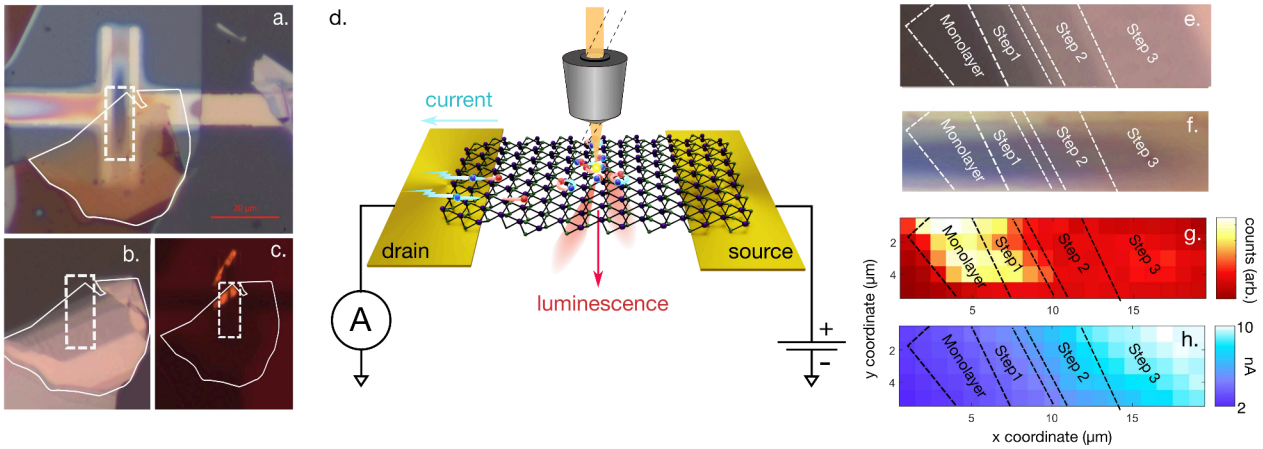

Figure 2. Separating bright and dark excitons through dual action spectroscopy mapping. A staircase flake, with multiple steps of increasing thickness from monolayer to bulk (bright field image in (b)), was mounted across two gold electrodes (a) on a sapphire substrate and encapsulated in hBN. It was ensured that a part of each thickness region made contact with both electrodes; monolayer contact is confirmed with fluorescence imaging in (c). The area of the sample that was mapped in this work is marked by dashed lines in (a), (b), and (c). A simplified experimental approach is shown in (d). Using a broad-band laser, the flake is illuminated with a 750 nm spot. The photoresponse is then measured by capturing both the fluorescence and photocurrent generated by the laser as the frequency components of the pulse are modulated. The excitation spectra are recovered through Fourier transform, and the process is repeated for each 1 × 1 μm portion of the flake to provide spatial resolution. The amplitude of the spectrum measured at each point is mapped in fluorescence (g) and photocurrent (h). The area of the flake that bridges the electrodes is cropped from (b). and thickness steps are labeled in (e). The same area of the sample is shown through bright-field microscopy in (f).

basis for exciton formation and propagation. Here, we untangle the roles of the bright **KK** exciton, dark **KK′** exciton, and dark **KΛ** exciton toward the photoresponse of WSe_2 at room temperature. To do so, we use microscopic broad-band Fourier transform excitation spectroscopy to spatially resolve the excitation spectrum of the material through two detection pathways.

A simplified schematic of the experimental approach is shown in Figure 2d. A WSe_2 staircase flake (a flake starting at monolayer thickness and increasing in steps up to bulk values) was mounted on a sapphire substrate across two gold electrodes (Figure 2a) and encapsulated with hBN. To obtain spectra, the frequency of a broad-band pulse was modulated in the Fourier domain. The PC response to illumination was monitored with a lockin amplifier where excitons are only detected once they reach the contact between the device and the active electrode, i.e., the electrode that supports conditions for charge tunneling and separation (more information in Supporting Information Figure 3). This means PC is only detected for excitons that diffuse from the point of illumination to the active electrode. PL was measured with a photon counting camera in transmission using a long-pass filter to block the illumination beam. The illumination was focused to a 750 nm spot and scanned across the flake with galvo mirrors so the spectrum of the WSe_2 could be resolved with microscopic spatial resolution. Maps, like the ones shown in Figure 2g,h, were then constructed for both detection mechanisms. Each pixel of these maps has a corresponding excitation spectrum for that specific part of the flake, indicated in Figure 2e,f. For those interested in reproducing the results here or using the experimental technique, a detailed explanation of the procedure is given in the Supporting Information. For all of the spectra presented here, true data points are shown, as well as a curve retrieved through zero padding and frequency filtering in the Fourier domain. Full descriptions of the data handling and the spectral acquisition process are also available in the Supporting Information.

The layer number of each step in the staircase is determined through absorption. The enhanced fluorescence in the thinnest section of the sample (Figure 2g) means we can confidently assign this section as a monolayer and use this absorption as a reference for the other layers. The absorption coefficients, plotted in Figure 3a, reveal the steps as 3, 6, and 12 layers (L) thick.

Spectra recovered in PL and PC show a clear distinction between exciton states more likely to recombine and states more likely to produce photocurrent in WSe_2. Figure 3b,c demonstrates this difference in the spectral ranges of 1.6−2.1 eV (780−590 nm), specifically at the band edge between 1.6−1.7 eV, that contains the transition energies between the VBM and the three conduction band valleys for the monolayer. In PL, a 40 meV red shift is visible with increasing thickness, shown in the inset of Figure 3c. The shift is indicative of relaxation of the bright state as splitting between spin states decreases at the K points. The red shift in PL is accompanied by a decrease in amplitude through 3L, 6L, and 12L. This is consistent with the quenching that occurs at multilayer thicknesses as electrons are funnelled toward the lower energy regions of the *k*-space, away from the allowed transition.

One such forbidden state dominates the exciton response in PC. Shown in Figure 3b, the **KK′** exciton peak (marked with a dashed line) remains fixed and red-shifted by ∼30 meV from the bright state in the monolayer throughout all thicknesses. Although all K points experience a shift in energy from introducing layers, the counteraction of spin−orbit coupling of electrons in the K′ minima and holes in the K maxima cancels out any overall change in the **KK′** resonance. Access to the momentum forbidden states in excitation is enabled through coupling to phonon modes at room temperature. The same access cannot be gained to the spin-forbidden exciton, as the likelihood of simultaneous photon absorption and spin flip is vanishingly small. We can conclude from these initial spectra that the photocurrent response of WSe_2 is dominated by momentum dark excitons. The forbidden transition required for recombination ensures longer lifetimes and a significantly

https://doi.org/10.1021/acs.nanolett.4c06349
Nano Lett. 2025, 25, 7658−7664

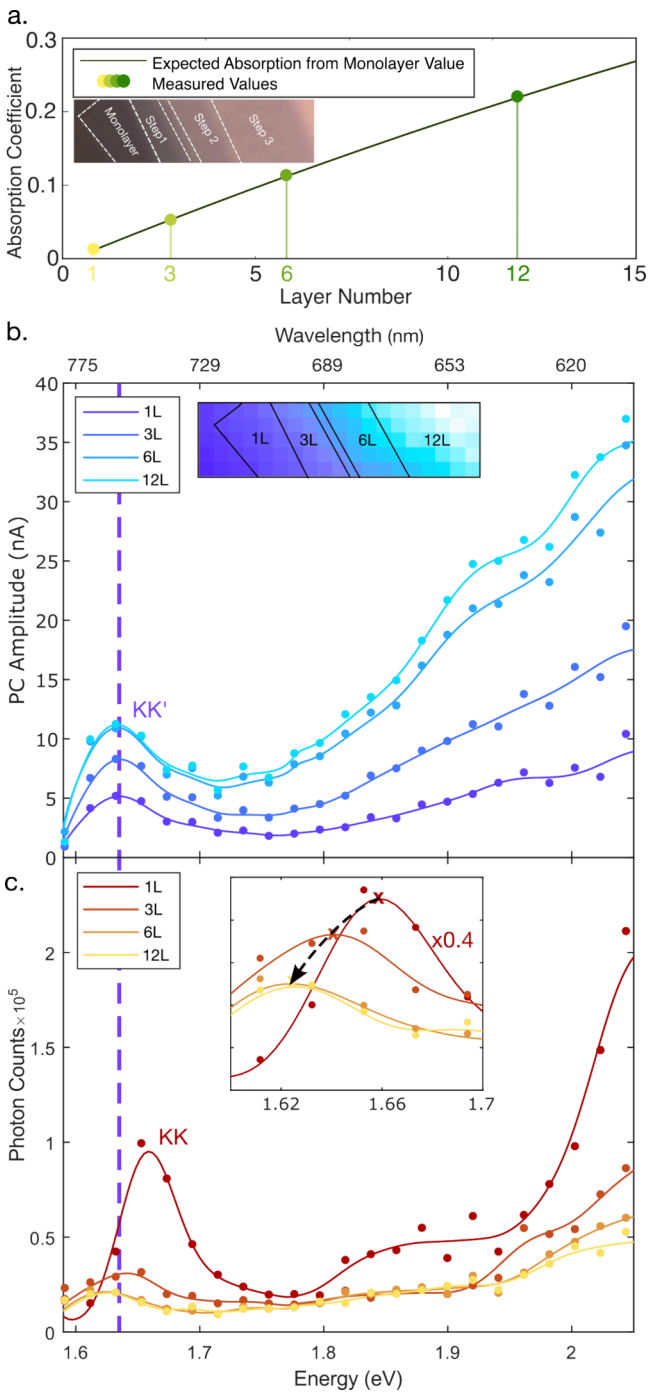

Figure 3. Absorption by step (a) and PC (b) and PL (c) excitation spectra for all 4 regions of the WSe_2 flake. In PL, the expected shift in both the spectral position and intensity of the bright exciton is observed (shown in the inset), as interlayer orbital overlap induces a red shift of the direct transition along with a switch in the ground state of the conduction band. In PC, we observe that the main exciton peak (marked with purple dashed line) directly corresponds to the literature value for the red shift of the dark **KK′** exciton.[9] No shift is observed in this exciton with layer thickness, while the amplitude of the peak saturates at this laser power (~20 μW) above the bilayer thickness.

greater chance to diffuse across the device. Lifetime may not be the only factor, as previous studies have established that the orbital character of each valley can vary dramatically, where in-plane orbitals (d_{xy}, $d_{x^2-y^2}$), that are expressed more in the momentum-dark valleys,[10] can contribute more effectively to transport. Naturally an increase in transport increases the likelihood of detection through PC, as the further an exciton diffuses, the higher the chance it has of reaching the potential barrier at the active electrode.

At this laser fluence (~1000 μJ cm^{-2}) saturation occurs in the state from 6 to 12 layers. An increase in signal is expected with added layers simply due to the increase in absorption, as observed in the blue part of each spectra, whereas the **KK′** transition approaches full saturation faster. We assign this effect to the enhanced dispersion efficiency that higher-energy excitations can access as they vibrationally relax to a conduction band minimum. Faster dispersion out of the interaction area would lead to a slower approach to saturation conditions. As alluded to in Figure 1, the CBM of multilayer WSe_2 lies at the **Λ** symmetry point, 200 meV below the **KK′** resonance. In order to inspect the bulk ground state dark exciton **KΛ**, we shifted the spectral excitation window to 1.4–1.7 eV (885–729 nm). Moving into this spectral window means that PL is no longer measurable, as the signal at wavelengths longer than 885 nm is below a detectable level at room temperature. The fluence was decreased to ~50 μJ cm^{-2} in these measurements to avoid saturation of the **KK′** state seen in Figure 3b. The fluence used in the PC-PL measurements was necessary to achieve the required signal-to-noise ratio in PL.

The excitation spectrum from 1.4 to 1.7 eV for each step of the flake is shown in Figure 4a. All multilayer steps show excitation peaks representing two momentum-forbidden states, the **KΛ** exciton at ~1.46 eV and the **KK′** exciton at 1.64 eV. The absence of the **KΛ** resonance in the monolayer spectrum is due to the dark states' degeneracy in 1L, in agreement with previous study.[8] The small redshift of 10 meV observed in the position of the ground state from 3L to 6L reflects further interlayer orbital overlap at multilayer thicknesses, where these effects become less pronounced as the band structure moves closer to that of the bulk material. There is significantly more off-resonance excitation in classical absorption spectra (Figure 4c) than in action spectra, obscuring the shape of the exciton peaks. The positions of all three excitons recorded across the excitation spectra are marked on the plot. The competition between the **KK** and **KK′** valleys is, for the most part, obscured by their near degeneracy at multilayer thicknesses. In the monolayer, two transitions are visible, while absorption in 3L, 6L, and 12L thicknesses falls off below 1.46 eV, inferring **KΛ** is the ground state exciton.

Notably, the inequality of amplitudes between the **KΛ** and **KK′** peaks across both spectral detection mechanisms indicates a greater probability of absorption into the K′ valley than the Λ. The curvature and width of each valley of interest will define the range of phonon momenta and photon energy with which an electron lying at the K point of the valence band can interact to access the conduction band valleys. The stability of each of these excitons can be gauged by the spatial dependence of their signal, relative to the active electrode. The amplitude of the overall PC signal is highly dependent on which electrode is used as active, an effect that is visible in Figure 4b. Leveraging this property, the spatial dependence of the spectra at each thickness is investigated in Figure 5.

The distance dependence of the PC excitation spectrum across the different thickness (Figure 5a,d) steps demonstrates the inequality in the stability between the two exciton states. The amplitude of the two exciton peaks with respect to

https://doi.org/10.1021/acs.nanolett.4c06349
Nano Lett. 2025, 25, 7658−7664

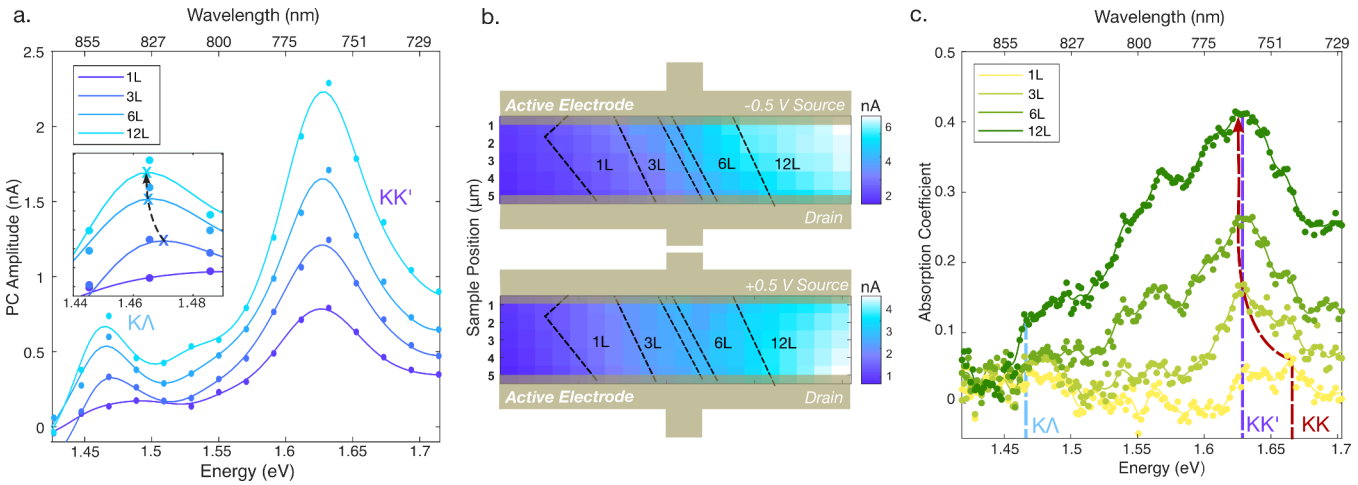

Figure 4. Momentum dark excitons of WSe_2. Appearance of the ground state dark exciton, **KΛ**, near 1.46 eV above monolayer thicknesses is shown in the PC signal of each region of the staircase, shown in (a). Absence of the peak in the monolayer region of the flake confirms the single WSe_2 layer, while we see a smaller red shift of the **KΛ** peak with thickness (shown inset) than that seen in PL.[18] The spectra in (a) are produced by averaging the signal from each region of the flake as shown in the top PC map in (b). Evidence of the position dependence of the signal is shown by flipping the location of the active electrode. Absorption measurements for each sample region (c) show that off-resonance absorption into exciton states is heavily filtered in the action spectra, while the peak of absorption follows the resonance of the bright exciton for each step.

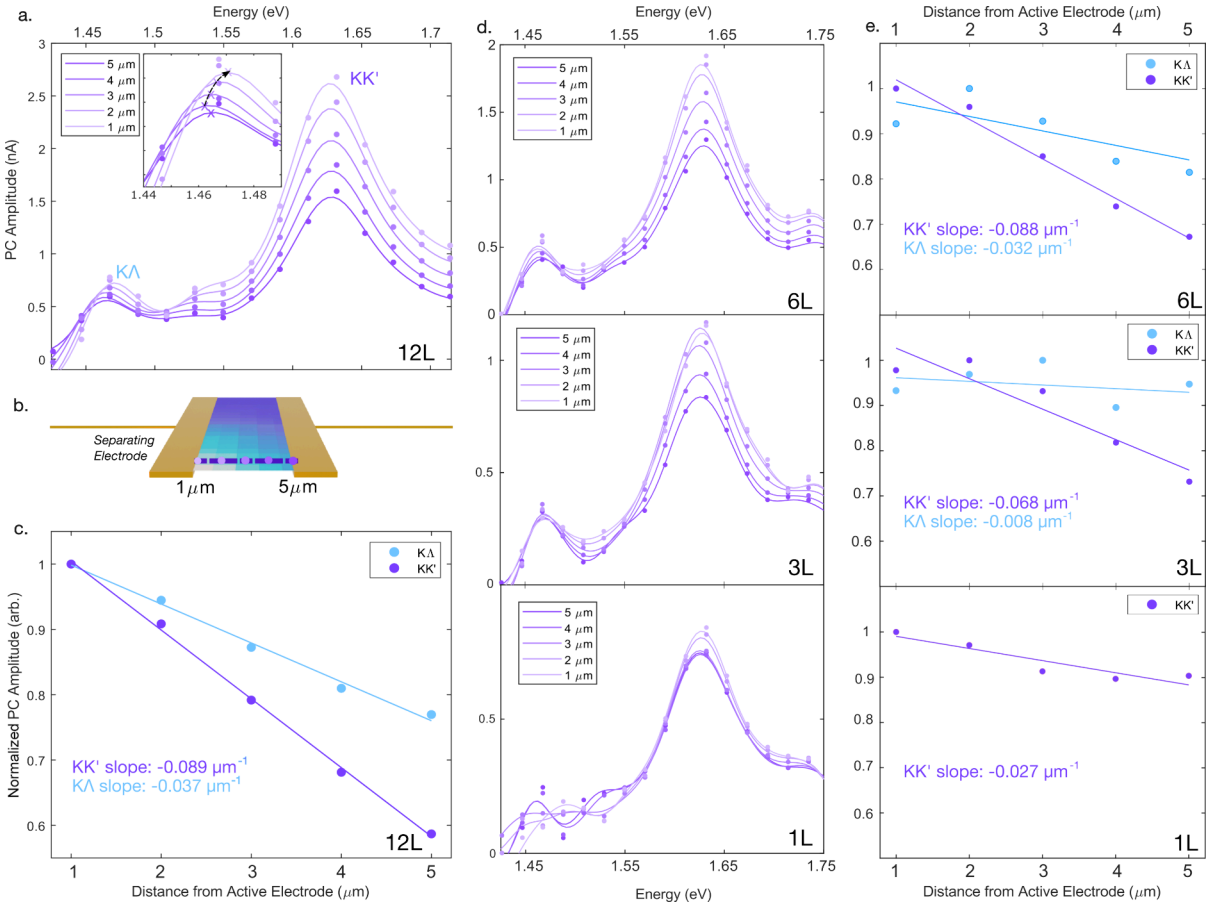

Figure 5. Diffusion of dark **KΛ** and **KK′** excitons. Mapping the sample spectrally (a,d) allows analysis of not only the spectra at different sample thicknesses but also the way the peaks change as excitons need to travel further to undergo charge separation. By isolating a cross section in the 12 layer part of the flake (marked with a dashed line in (b)) and stacking the plots (a), the spectral transformation is clear when moving the point of illumination away from the active electrode. Overall the amplitude of both states increases toward the electrode. The normalized slope of this increase is shown for each exciton in (c) for 12 L and (e) for all others. The **KΛ** exciton is lower in amplitude across all spectra than the **KK′**, but its spatial decay is lower, implying greater stability and more effective diffusion. Moving to fewer layers, the stability of both excitons across the device increases, with almost no change in amplitude in **KΛ** in 3L and **KK′** in the monolayer, respectively.

https://doi.org/10.1021/acs.nanolett.4c06349
Nano Lett. 2025, 25, 7658−7664

electrode distance is normalized and plotted in Figure 5c for 12L and Figure 5e for all other thicknesses. Although the ground state has a smaller overall contribution to the PC signal, it is more stable than the **KK′** exciton in space. Extrapolating from the lines drawn in Figure 5c, we can estimate that the photocurrent signal could be drawn from each exciton peak over distances of 10 and 20 μm for **KK′** and **KΛ**, respectively. Although enhanced exciton−exciton annihilation in the more densely populated valley may contribute to the inequality, both the linear nature of the signal degradation and increase in stability of both states at fewer layers imply annihilation is not dominant in the decay. The **KΛ** amplitude is almost unchanged over the device at a 3L thickness. The apparent stability but small amplitude of the **KΛ** exciton points toward the inaccessibility of the electronic transition needed for both recombination and excitation. Theoretical work on monolayer WSe_2 predicts different diffusion constants for different effective valley masses,[38] which could also point to the behavior that we see here. This study predicted intervalley coupling in the monolayer at room temperature, leading to an averaging of the diffusion constant, given the near degeneracy of the three valleys in the single-layer structure of the material. Probing deeper into the bulk, we observe that the energetic barriers introduced in the multilayer band structure inhibit the same degree of intervalley coupling, which presents an opportunity to use such a difference in diffusivity. This property opens the door for many promising applications in novel electronics, leveraging the valley polarization available in these materials, over lengths far beyond what's needed in modern devices. Room-temperature measurements of valley bias in TMDs bring the potential of utilizing valleytronics in working devices away from the confines of cryogenic conditions. Moving to an environment rich in thermal energy, we have shown that while the myriad of states available in the low temperature regime disappears, the momentum forbidden dark excitons not only remain stable at room temperature but dominate the photoelectric response of the material over many micrometers.

We have presented a novel technique for the detection and diagnosis of energy transfer in photoactive materials. We demonstrate that in the presence of both bright and dark excitons, the photocurrent response of WSe_2 is dominated by the dark **KK′** state, which acts as the main state for the propagation of energy more generally. We also observed that although the ground state exciton, **KΛ**, contributes less to the exciton population, its inaccessibility in transition leads to stability, which manifests into diffusion over tens of micrometers. The relative simplicity of the experimental approach paves the way for further studies of energy transfer in photoactive materials, which brings the reality of valleytronics applications a step closer.

■ ASSOCIATED CONTENT

Supporting Information

The Supporting Information is available free of charge at https://pubs.acs.org/doi/10.1021/acs.nanolett.4c06349.

■ AUTHOR INFORMATION

Corresponding Authors

Joseph Wragg − *ICFO - Institut de Ciencies Fotoniques, The Barcelona Institute of Science and Technology, Castelldefels, Barcelona 08860, Spain*; Email: joseph.wragg@icfo.eu

Niek F. van Hulst − *ICFO - Institut de Ciencies Fotoniques, The Barcelona Institute of Science and Technology, Castelldefels, Barcelona 08860, Spain; ICREA, Institució Catalana de Recerca i Estudis Avançats, Barcelona, Spain. 08010;* orcid.org/0000-0003-4630-1776; Email: niek.vanhulst@icfo.eu

Authors

Luca Bolzonello − *ICFO - Institut de Ciencies Fotoniques, The Barcelona Institute of Science and Technology, Castelldefels, Barcelona 08860, Spain;* orcid.org/0000-0003-0893-5743

Ludovica Donati − *LENS, European Laboratory for Non-Linear Spectroscopy, 50019 Sesto Fiorentino FI, Italy*

Karuppasamy Pandian Soundarapandian − *ICFO - Institut de Ciencies Fotoniques, The Barcelona Institute of Science and Technology, Castelldefels, Barcelona 08860, Spain;* orcid.org/0000-0002-9664-9095

Riccardo Bertini − *ICFO - Institut de Ciencies Fotoniques, The Barcelona Institute of Science and Technology, Castelldefels, Barcelona 08860, Spain*

Seth Ariel Tongay − *SEMTE, The School for Engineering of Matter, Transport and Energy, Arizona State University, Tempe, AZ 85287, United States;* orcid.org/0000-0001-8294-984X

Kenji Watanabe − *National Institute for Materials Science, Tsukuba 305-0047 Ibaraki, Japan;* orcid.org/0000-0003-3701-8119

Takashi Taniguchi − *National Institute for Materials Science, Tsukuba 305-0047 Ibaraki, Japan;* orcid.org/0000-0002-1467-3105

Frank H. L. Koppens − *ICFO - Institut de Ciencies Fotoniques, The Barcelona Institute of Science and Technology, Castelldefels, Barcelona 08860, Spain; ICREA, Institució Catalana de Recerca i Estudis Avançats, Barcelona, Spain. 08010;* orcid.org/0000-0001-9764-6120

Complete contact information is available at: https://pubs.acs.org/10.1021/acs.nanolett.4c06349

Notes

The authors declare no competing financial interest.

■ ACKNOWLEDGMENTS

J.W., L.B., and N.F.v.H. acknowledge support through the MCIN/AEI projects PID2021-123814OB-I00, TED2021-129241BI00, the "Severo Ochoa" program for Centres of Excellence in R&D CEX2019-000910-S, Fundacio Privada Cellex, Fundacio Privada Mir-Puig, and the Generalitat de Catalunya through the CERCA program. N.F.v.H. acknowledges financial support from the European Commission (ERC Advanced Grant 101054846-FastTrack). This work is part of the ICFO Clean Planet Program supported by Fundació Joan Ribas Araquistain (FJRA).

■ REFERENCES

(1) Baldereschi, A.; Lipari, N. C. Energy levels of direct excitons in semiconductors with degenerate bands. *Phys. Rev. B* **1971**, *3*, 439.

(2) Laussy, F. P.; Kavokin, A. V.; Shelykh, I. A. Exciton-polariton mediated superconductivity. *Physical review letters* **2010**, *104*, 106402.

(3) Hu, J.; Lorchat, E.; Chen, X.; Watanabe, K.; Taniguchi, T.; Heinz, T. F.; Murthy, P. A.; Chervy, T. Quantum control of exciton wave functions in 2D semiconductors. Science Advances. *Science Advances* **2024**, *10*, eadk6369.

(4) Mueller, T.; Malic, E. Exciton physics and device application of two-dimensional transition metal dichalcogenide semiconductors. *npj 2D Materials and Applications* **2018**, *2*, 29.
(5) Yan, T.; Qiao, X.; Liu, X.; Tan, P.; Zhang, X. Photoluminescence properties and exciton dynamics in monolayer WSe2. *Appl. Phys. Lett.* **2014**, *105*, 101901.
(6) He, K.; Kumar, N.; Zhao, L.; Wang, Z.; Mak, K. F.; Zhao, H.; Shan, J. Tightly bound excitons in monolayer WSe 2. *Physical review letters* **2014**, *113*, 026803.
(7) Hanbicki, A.; Currie, M.; Kioseoglou, G.; Friedman, A.; Jonker, B. Measurement of high exciton binding energy in the monolayer transition-metal dichalcogenides WS2 and WSe2. *Solid State Commun.* **2015**, *203*, 16−20.
(8) Kumar, A.; Ahluwalia, P. Electronic structure of transition metal dichalcogenides monolayers 1H-MX 2 (M= Mo, W; X= S, Se, Te) from ab-initio theory: new direct band gap semiconductors. *European Physical Journal B* **2012**, *85*, 1−7.
(9) Deilmann, T.; Thygesen, K. S. Finite-momentum exciton landscape in mono-and bilayer transition metal dichalcogenides. *2D Materials* **2019**, *6*, 035003.
(10) Riley, J. M.; Mazzola, F.; Dendzik, M.; Michiardi, M.; Takayama, T.; Bawden, L.; Granerød, C.; Leandersson, M.; Balasubramanian, T.; Hoesch, M.; et al. Direct observation of spin-polarized bulk bands in an inversion-symmetric semiconductor. *Nat. Phys.* **2014**, *10*, 835−839.
(11) Shahnazaryan, V.; Iorsh, I.; Shelykh, I. A.; Kyriienko, O. Exciton-exciton interaction in transition-metal dichalcogenide monolayers. *Phys. Rev. B* **2017**, *96*, 115409.
(12) Erkensten, D.; Brem, S.; Malic, E. Exciton-exciton interaction in transition metal dichalcogenide monolayers and van der Waals heterostructures. *Phys. Rev. B* **2021**, *103*, 045426.
(13) Regan, E. C.; Wang, D.; Paik, E. Y.; Zeng, Y.; Zhang, L.; Zhu, J.; MacDonald, A. H.; Deng, H.; Wang, F. Emerging exciton physics in transition metal dichalcogenide heterobilayers. *Nature Reviews Materials* **2022**, *7*, 778−795.
(14) Robert, C.; Lagarde, D.; Cadiz, F.; Wang, G.; Lassagne, B.; Amand, T.; Balocchi, A.; Renucci, P.; Tongay, S.; Urbaszek, B.; et al. Exciton radiative lifetime in transition metal dichalcogenide monolayers. *Phys. Rev. B* **2016**, *93*, 205423.
(15) Koperski, M.; Nogajewski, K.; Arora, A.; Cherkez, V.; Mallet, P.; Veuillen, J.-Y.; Marcus, J.; Kossacki, P.; Potemski, M. Single photon emitters in exfoliated WSe2 structures. *Nature Nanotechnol.* **2015**, *10*, 503−506.
(16) Splendiani, A.; Sun, L.; Zhang, Y.; Li, T.; Kim, J.; Chim, C.-Y.; Galli, G.; Wang, F. Emerging photoluminescence in monolayer MoS2. *Nano Lett.* **2010**, *10*, 1271−1275.
(17) Mak, K. F.; Lee, C.; Hone, J.; Shan, J.; Heinz, T. F. Atomically thin MoS 2: a new direct-gap semiconductor. *Physical review letters* **2010**, *105*, 136805.
(18) Zhao, W.; Ghorannevis, Z.; Chu, L.; Toh, M.; Kloc, C.; Tan, P.-H.; Eda, G. Evolution of electronic structure in atomically thin sheets of WS2 and WSe2. *ACS Nano* **2013**, *7*, 791−797.
(19) Zhang, X.-X.; You, Y.; Zhao, S. Y. F.; Heinz, T. F. Experimental evidence for dark excitons in monolayer WSe 2. *Physical review letters* **2015**, *115*, 257403.
(20) Ersfeld, M.; Volmer, F.; Rathmann, L.; Kotewitz, L.; Heithoff, M.; Lohmann, M.; Yang, B.; Watanabe, K.; Taniguchi, T.; Bartels, L.; et al. Unveiling valley lifetimes of free charge carriers in monolayer WSe2. *Nano Lett.* **2020**, *20*, 3147−3154.
(21) Tang, Y.; Mak, K. F.; Shan, J. Long valley lifetime of dark excitons in single-layer WSe2. *Nat. Commun.* **2019**, *10*, 4047.
(22) Chand, S. B.; Woods, J. M.; Quan, J.; Mejia, E.; Taniguchi, T.; Watanabe, K.; Alù, A.; Grosso, G. Interaction-driven transport of dark excitons in 2D semiconductors with phonon-mediated optical readout. *Nat. Commun.* **2023**, *14*, 3712.
(23) Madéo, J.; Man, M. K.; Sahoo, C.; Campbell, M.; Pareek, V.; Wong, E. L.; Al-Mahboob, A.; Chan, N. S.; Karmakar, A.; Mariserla, B. M. K.; et al. Directly visualizing the momentum-forbidden dark excitons and their dynamics in atomically thin semiconductors. *Science* **2020**, *370*, 1199−1204.
(24) Lindlau, J.; Selig, M.; Neumann, A.; Colombier, L.; Förste, J.; Funk, V.; Förg, M.; Kim, J.; Berghäuser, G.; Taniguchi, T.; et al. The role of momentum-dark excitons in the elementary optical response of bilayer WSe2. *Nat. Commun.* **2018**, *9*, 2586.
(25) Ye, Z.; Cao, T.; O'brien, K.; Zhu, H.; Yin, X.; Wang, Y.; Louie, S. G.; Zhang, X. Probing excitonic dark states in single-layer tungsten disulphide. *Nature* **2014**, *513*, 214−218.
(26) Li, Z.; Wang, T.; Miao, S.; Li, Y.; Lu, Z.; Jin, C.; Lian, Z.; Meng, Y.; Blei, M.; Taniguchi, T.; et al. Phonon-exciton Interactions in WSe2 under a quantizing magnetic field. *Nat. Commun.* **2020**, *11*, 3104.
(27) Zhang, X.-X.; Cao, T.; Lu, Z.; Lin, Y.-C.; Zhang, F.; Wang, Y.; Li, Z.; Hone, J. C.; Robinson, J. A.; Smirnov, D.; et al. Magnetic brightening and control of dark excitons in monolayer WSe2. *Nature Nanotechnol.* **2017**, *12*, 883−888.
(28) Park, K.-D.; Jiang, T.; Clark, G.; Xu, X.; Raschke, M. B. Radiative control of dark excitons at room temperature by nano-optical antenna-tip Purcell effect. *Nature Nanotechnol.* **2018**, *13*, 59−64.
(29) Vasconcelos, R.; Braganca, H.; Qu, F.; Fu, J. Dark exciton brightening and its engaged valley dynamics in monolayer wse 2. *Phys. Rev. B* **2018**, *98*, 195302.
(30) Zhou, Y.; Scuri, G.; Wild, D. S.; High, A. A.; Dibos, A.; Jauregui, L. A.; Shu, C.; De Greve, K.; Pistunova, K.; Joe, A. Y.; et al. Probing dark excitons in atomically thin semiconductors via near-field coupling to surface plasmon polaritons. *Nature Nanotechnol.* **2017**, *12*, 856−860.
(31) Quereda, J.; Ghiasi, T. S.; Van Zwol, F. A.; Van der Wal, C. H.; Van Wees, B. J. Observation of bright and dark exciton transitions in monolayer MoSe2 by photocurrent spectroscopy. *2D Materials* **2018**, *5*, 015004.
(32) Rahaman, M.; Selyshchev, O.; Pan, Y.; Schwartz, R.; Milekhin, I.; Sharma, A.; Salvan, G.; Gemming, S.; Korn, T.; Zahn, D. R. Observation of Room-Temperature Dark Exciton Emission in Nanopatch-Decorated Monolayer WSe2 on Metal Substrate. Advanced. *Opt. Mater.* **2021**, *9*, 2101801.
(33) Gelly, R. J.; Renaud, D.; Liao, X.; Pingault, B.; Bogdanovic, S.; Scuri, G.; Watanabe, K.; Taniguchi, T.; Urbaszek, B.; Park, H.; et al. Probing dark exciton navigation through a local strain landscape in a WSe2 monolayer. *Nat. Commun.* **2022**, *13*, 232.
(34) Baranowski, M.; Surrente, A.; Maude, D. K.; Ballottin, M.; Mitioglu, A.; Christianen, P. C.; Kung, Y.-C.; Dumcenco, D.; Kis, A.; Plochocka, P. Dark excitons and the elusive valley polarization in transition metal dichalcogenides. *2D Materials* **2017**, *4*, 025016.
(35) Ciarrocchi, A.; Tagarelli, F.; Avsar, A.; Kis, A. Excitonic devices with van der Waals heterostructures: valleytronics meets twistronics. *Nature Reviews Materials* **2022**, *7*, 449−464.
(36) Lindlau, J.; Selig, M.; Neumann, A.; Colombier, L.; Förste, J.; Funk, V.; Förg, M.; Kim, J.; Berghäuser, G.; Taniguchi, T.; et al. The role of momentum-dark excitons in the elementary optical response of bilayer WSe2. *Nat. Commun.* **2018**, *9*, 2586.
(37) Le, D.; Barinov, A.; Preciado, E.; Isarraraz, M.; Tanabe, I.; Komesu, T.; Troha, C.; Bartels, L.; Rahman, T. S.; Dowben, P. A. Spin-orbit coupling in the band structure of monolayer WSe2. *J. Phys.: Condens. Matter* **2015**, *27*, 182201.
(38) Rosati, R.; Perea-Causín, R.; Brem, S.; Malic, E. Negative effective excitonic diffusion in monolayer transition metal dichalcogenides. *Nanoscale* **2020**, *12*, 356−363.

https://doi.org/10.1021/acs.nanolett.4c06349
Nano Lett. 2025, 25, 7658−7664